Journal of Advanced Ceramics
2020, **9**(6): 759–768
https://doi.org/10.1007/s40145-020-0412-7

ISSN 2226-4108
CN 10-1154/TQ

Research Article

Synthesis, microstructure, and properties of high purity Mo_2TiAlC_2 ceramics fabricated by spark plasma sintering

Yunhui NIU[a,†], Shuai FU[b,†], Kuibao ZHANG[a], Bo DAI[a], Haibin ZHANG[c], Salvatore GRASSO[b], Chunfeng HU[b,*]

[a]*State Key Laboratory of Environment-Friendly Energy Materials, Southwest University of Science and Technology, Mianyang 621010, China*
[b]*Key Laboratory of Advanced Technologies of Materials, Ministry of Education, School of Materials Science and Engineering, Southwest Jiaotong University, Chengdu 610031, China*
[c]*Institute of Nuclear Physics and Chemistry, China Academy of Engineering Physics, Mianyang 621900, China*

Received: May 12, 2020; Revised: August 13, 2020; Accepted: August 14, 2020

Abstract: The synthesis, microstructure, and properties of high purity dense bulk Mo_2TiAlC_2 ceramics were studied. High purity Mo_2TiAlC_2 powder was synthesized at 1873 K starting from Mo, Ti, Al, and graphite powders with a molar ratio of 2:1:1.25:2. The synthesis mechanism of Mo_2TiAlC_2 was explored by analyzing the compositions of samples sintered at different temperatures. It was found that the Mo_2TiAlC_2 phase was formed from the reaction among Mo_3Al_2C, Mo_2C, TiC, and C. Dense Mo_2TiAlC_2 bulk sample was prepared by spark plasma sintering (SPS) at 1673 K under a pressure of 40 MPa. The relative density of the dense sample was 98.3%. The mean grain size was 3.5 μm in length and 1.5 μm in width. The typical layered structure could be clearly observed. The electrical conductivity of Mo_2TiAlC_2 ceramic measured at the temperature range of 2–300 K decreased from 0.95×10^6 to 0.77×10^6 $\Omega^{-1}\cdot m^{-1}$. Thermal conductivity measured at the temperature range of 300–1273 K decreased from 8.0 to 6.4 $W\cdot(m\cdot K)^{-1}$. The thermal expansion coefficient (TEC) of Mo_2TiAlC_2 measured at the temperature of 350–1100 K was calculated as 9.0×10^{-6} K^{-1}. Additionally, the layered structure and fine grain size benefited for excellent mechanical properties of low intrinsic Vickers hardness of 5.2 GPa, high flexural strength of 407.9 MPa, high fracture toughness of 6.5 $MPa\cdot m^{1/2}$, and high compressive strength of 1079 MPa. Even at the indentation load of 300 N, the residual flexural strength could hold 84% of the value of undamaged one, indicating remarkable damage tolerance. Furthermore, it was confirmed that Mo_2TiAlC_2 ceramic had a good oxidation resistance below 1200 K in the air.

Keywords: MAX phase; Mo_2TiAlC_2; synthesis; microstructure; properties

1 Introduction

In recent years, MAX phases of ternary layered compounds have attracted much attention from material scientists in the world owing to their excellent combining properties of ceramics and metals. The formula of MAX phases could be presented as $M_{n+1}AX_n$, where M is a transition metal, A is an A group element, X is carbon or nitrogen, and n = 1–6 [1–15]. The research results have shown that the MAX phases possess good

† Yunhui Niu and Shuai Fu contributed equally to this work.
* Corresponding author.
E-mail: chfhu@live.cn

electrical and thermal conductivities, low hardness, normal thermal expansion coefficient (TEC), high damage tolerance, and thermal shock resistance, being the candidates applied in the industrial and aerospace fields [16–31].

In the MAX phase family, there is one kind of solid solutions of $(M',M'')_{n+1}AX_n$ where the M site is composed of two elements, and they have the possible multiple properties of $M'_{n+1}AX_n$ and $M''_{n+1}AX_n$, triggering the interests of researchers. By controlling the solid solute elements, new MAX phases-compounds could also be synthesized. For example, Sun *et al*. [32–36] successfully prepared $(V_{0.5}Cr_{0.5})_3AlC_2$, $(V_{0.5}Cr_{0.5})_4AlC_3$, and $(V_{0.5}Cr_{0.5})_5Al_2C_3$ MAX phases by using *in situ* reaction method and found that these phases had the good high-temperature stiffness of V-based MAX phase and the good hot corrosion resistance of Cr-based MAX phase. Zheng *et al*. [37] synthesized $(Ti_{0.5}Nb_{0.5})_5AlC_4$ compound which is the first layered 514 phase, therefore improving the discovery of more new MAX phases. In recent years, Anasori *et al*. [38,39] identified two new solid solution MAX phases of Mo_2TiAlC_2 and $Mo_2Ti_2AlC_3$ and determined the order arrangement of Mo atom layer and Ti atom layer in the crystal structure. Also, Fu *et al.* [40] synthesized high purity dense $Mo_2Ti_2AlC_3$ sample with a relative density of 99.3% by the hot pressing method and systematically characterized its physical and mechanical properties. Fu *et al*. [40] confirmed that $Mo_2Ti_2AlC_3$ ceramic has the lowest thermal conductivity of 6.82 $W\cdot(m\cdot K)^{-1}$ in the known MAX phases. Whereas, until 2020, except for Refs. [38,39], the experimental researches on the basic physical and mechanical properties of Mo_2TiAlC_2 were quiet rare.

Additionally, in order to fabricate the dense Mo_2TiAlC_2 ceramics with fine grains, spark plasma sintering (SPS) was adopted based on the merits of on-off DC pulse current to generate discharge plasma, releasing point impact pressure and Joule heat, and accelerating electric field diffusion [41–44]. In previous studies, SPS method has been well utilized to successfully prepare MAX phases of Ti_2AlC [45], Ti_2AlN [46], Ta_4AlC_3 [47], Ti_2SnC [48], and Cr_2AlC [49]. The good characteristics of fast heating, shortening annealing time, and high production efficiency have been well proved. Especially, under the condition of short annealing time and high pressure, it is convenient to achieve fine grains in the dense bulks, benefiting for the good mechanical properties.

In this paper, high purity Mo_2TiAlC_2 powders were synthesized firstly and its reaction mechanism was systematically investigated. Dense Mo_2TiAlC_2 ceramics were consolidated by SPS and their physical and mechanical properties, as well as oxidation resistance, were studied.

2 Experimental

The preparation of high purity dense Mo_2TiAlC_2 ceramics was divided into two steps: One step was to explore the reaction mechanisms to synthesize high purity Mo_2TiAlC_2 powders, and the second step was to consolidate the dense bulks by SPS. For the synthesis of high purity powders, commercial powders of Mo (300 mesh, 99% purity), Ti (200 mesh, 99.5% purity), Al (300 mesh, 99% purity), and graphite (1500 mesh, 99% purity) were used as initial materials. The designed molar ratio of Mo:Ti:Al:C was 2:1:1.25:2. The adding excessive aluminum was to compensate for the evaporation of Al during high-temperature treatment. The raw powders were weighed in an electric balance with an accuracy of 10^{-2} g and drily mixed in a resin bottle at 50 rpm in a rotary milling machine for 20 h. After sieving, the mixture was filled in an alumina crucible and sintered in the tube furnace (BR-17MT, Brother Co., Ltd., China) at the aimed temperature in a flowing argon atmosphere (99.9% purity). The heating and cooling rate was 5 K/min and the holding time was 4 h. In order to synthesize pure Mo_2TiAlC_2 powders, the reaction mechanisms of Mo_2TiAlC_2 ceramic were systematically investigated at the temperatures of 300, 973, 1273, 1573, and 1873 K, respectively. After sintering, the powders were drilled from the specimens and sieved using a 200 mesh sieve. The compositions of obtained fine powders were examined by a D8 Bruker X-ray diffractometer (XRD) (PA, Almelo, the Netherlands) with Cu Kα (λ = 1.54178 Å). Finally, it was confirmed that the pure Mo_2TiAlC_2 powder could be successfully prepared at 1873 K.

For fabricating the dense Mo_2TiAlC_2 ceramics, the high purity powders with the particle size of 200 mesh were put into a graphite mold with a diameter of 20 mm and consolidated at 1673 K in a SPS furnace (SPS-20T-10, Chenhua Co., Ltd., China) in a vacuum (1 Pa) under a pressure of 40 MPa and then the samples were cooled down to the ambient temperature naturally. The heating rate was 20 K/min and the

holding time was 10 min. Finally, the dense samples were ground to remove the surface contaminations by a diamond grinding wheel. Phase constituents of the sample were examined by XRD, and the density of the sample was measured by the Archimedes' method. After etching the polished surface of Mo_2TiAlC_2 ceramics using the acid solution consisting of HNO_3, HF, and H_2O with the volume ratio of 1:1:1, the grains were carefully checked by a scanning electron microscope (FEI, Hillaboro Co., USA) equipped with an energy-dispersive X-ray spectroscopy (EDS). At least 50 grains were measured in length and width.

The electrical conductivity was measured by physical property measurement system (PPMS DynaCool 9, Quantum Design Co., USA) at the temperature range of 2–300 K. The sample size used was 3 mm × 3 mm × 15 mm. The thermal conductivity was measured by a hot disk method (TPS2500, Hot Disk Co., Sweden) at the temperatures of 300, 473, 673, 873, 1073, and 1273 K, respectively. The sample used for testing thermal conductivity was a cylinder with a 20 mm diameter and 5 mm height. The TEC was measured using a thermal expansion analyzer (DIL402C, Netzsch Co., Germany) at the temperature range of 350–1100 K in flowing argon. The heating rate was set at 1.5 K/min, and the dimension of the sample was 3 mm × 4 mm × 4 mm.

The Vickers hardness was tested in a micro-hardness tester (HVS-50, Wheng Co., China), and the loads were selected as 1, 2, 3, 5, 10, 50, and 100 N, respectively. An universal testing machine (YC-100KN, Yice Co., China) was used to determinate the mechanical properties, including fracture toughness (crosshead speed, 0.05 mm/min), flexural strength (crosshead speed, 0.5 mm/min), and compressive strength (crosshead speed, 0.5 mm/min). The specimens were machined into bars with the dimensions of 2 mm × 4 mm × 18 mm, 1.5 mm × 2 mm × 18 mm, and 2 mm × 2 mm × 4 mm respectively by an electrical-discharged method and then polished down to 1.0 μm diamond grits. The notch of the samples for the fracture toughness test was 2 mm in length and 0.2 mm in width. The testing span of three-point bending strength and the fracture toughness was 16 mm. Three samples were used for each test. The damage tolerance of Mo_2TiAlC_2 ceramics was characterized by the indentation load dependence of flexural strength, and the indentation loads selected were 0, 10, 50, 100, 200, and 300 N, respectively. The fracture surface was observed by scanning electron microscope (SEM).

In addition, in order to determine the oxidation resistance of Mo_2TiAlC_2 ceramics, the DSC–TG curve was evaluated by a TG–DSC facility (STA 449F3, Netzsch Corp., Germany) at the temperature range of 313–1473 K. The heating rate was 20 K/min and the flowing rate of air was 20 ml/min. Furthermore, the dense Mo_2TiAlC_2 sample with the dimension of 1.5 mm × 2 mm × 5 mm was heat-treated in the tube furnace in the air from room temperature to 1473 K at the heating rate of 10 K/min. The oxidized surface was examined by XRD and SEM.

3 Results and discussion

3.1 Synthesis and microstructure characterization

In order to explore the reaction mechanisms of Mo_2TiAlC_2 and synthesize pure Mo_2TiAlC_2 powder, the sintering was processed at different temperatures. The XRD results of the obtained phases are shown in Fig. 1. The compositions in the prepared samples were listed in Table 1. The temperatures corresponding to Figs. 1(a)–1(e) are 300, 973, 1273, 1573, and 1873 K, respectively. In comparison with the initial compositions of mixture powder at 300 K (Fig. 1(a)), no reaction occurred at 973 K, and only element powders could be examined (Fig. 1(b)). When raising the temperature to 1273 K, a large amount of Al and Mo reacted and generated the main phase of $AlMo_3$ (Fig. 1(c)). In addition, a small amount of $AlTi_3$ and Mo_2C were detected. The chemical reaction equations could be expressed as

$$Al + 3Mo = AlMo_3 \quad (1)$$

$$Al + 3Ti = AlTi_3 \quad (2)$$

$$2Mo + C = Mo_2C \quad (3)$$

As the temperature reached 1573 K, the diffraction peak intensity of $AlMo_3$ decreased a lot and the $AlTi_3$ phase disappeared, whereas the diffraction peak intensity of Mo_2C continued to increase to be the main phase, indicating the continuous reaction between Mo and C (Fig. 1(d)). Additionally, plenty of Mo_3Al_2C, a small amount of TiC, and a few Mo_2TiAlC_2 were examined. At the same time, graphite was also reacted. It is suspected that the consumption of $AlMo_3$, $AlTi_3$, and C probably contributed to the formation of Mo_3Al_2C and TiC. When further increasing the temperature to be 1873 K, all phases of C, $AlMo_3$, Mo_2C, Mo_3Al_2C, and

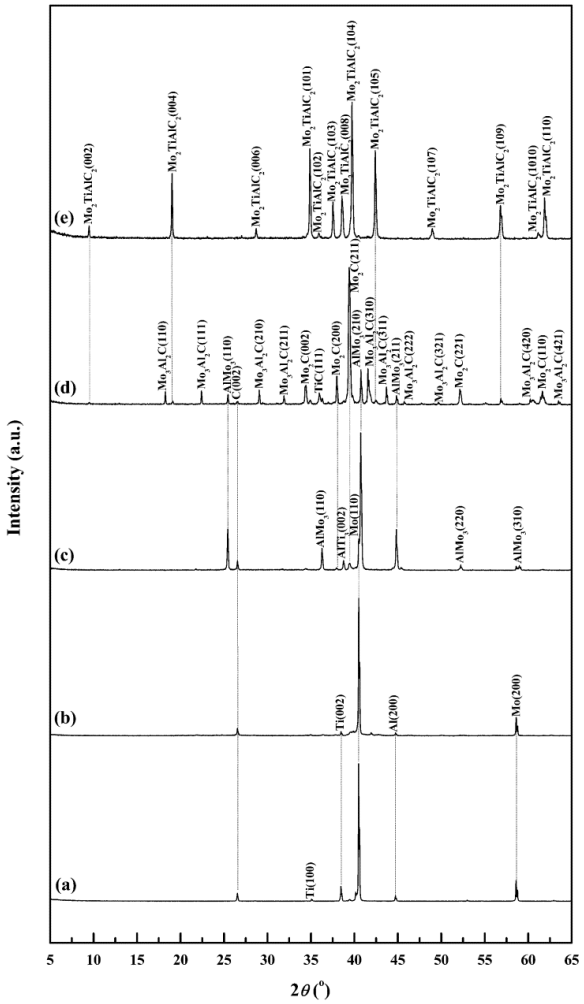

Fig. 1 XRD patterns of synthesized specimens sintered at different temperatures: (a) 300, (b) 973, (c) 1273, (d) 1573, and (e) 1873 K.

Table 1 Phase compositions of samples sintered at different temperature

Temperature (K)	Phase composition
300	Mo, Ti, Al, C
973	Mo, Ti, Al, C
1273	Mo, C, $AlMo_3$, Mo_2C, $AlTi_3$
1573	C, $AlMo_3$, Mo_2C, Mo_3Al_2C, TiC, Mo_2TiAlC_2
1873	Mo_2TiAlC_2

TiC disappeared and only Mo_2TiAlC_2 could be examined (Fig. 1(e)). So, the newly formed phases of Mo_3Al_2C and TiC possibly reacted with Mo_2C to form Mo_2TiAlC_2. Therefore, the chemical reaction equations could be expressed as

$$8AlMo_3 + 4AlTi_3 + 21C = 6Mo_3Al_2C + 12TiC + 3Mo_2C \quad (4)$$

$$2Mo_3Al_2C + 4TiC + Mo_2C + C = 4Mo_2TiAlC_2 \quad (5)$$

As a result, it could be determined that high purity Mo_2TiAlC_2 powder could be successfully synthesized at 1873 K with the molar ratio of Mo:Ti:Al:C of 2:1:1.25:2.

Figure 2 shows the XRD patterns of the dense Mo_2TiAlC_2 bulks and pure Mo_2TiAlC_2 powder. It is detected that after consolidation by SPS, the obtained dense Mo_2TiAlC_2 ceramics still kept high purity with almost no impurity. The diffraction peaks of (002), (004), (006), and (008) became stronger in the dense specimens in comparison with those of initial fine Mo_2TiAlC_2 particles. It is concluded that during the sintering process, the growth of Mo_2TiAlC_2 grains showed the preferential direction with the *c*-axis of grains parallel to the loading direction under high pressures. A similar result has been previously reported on Ti_2AlN ceramic densified by SPS, which was ascribed to the mechanical oriented deformation [50].

The microstructure characterization of dense Mo_2TiAlC_2 ceramics was shown in Fig. 3. In the etched surface of Mo_2TiAlC_2 ceramics, plate-like grains with random orientation could be clearly observed (Fig. 3(a)). By measuring the length and width of at least 50 grains, the mean grain size was calculated to be 3.5 μm in length and 1.0 μm in width, which is finer than those of $Mo_2Ti_2AlC_3$ (5 μm in length and 1.3 μm in width) [40]. The smaller grain size is probably ascribed to the SPS sintering method which supplies a high heating rate and short annealing time to effectively inhibit the rapid grain growth. Figure 3(b) shows the fracture surface of Mo_2TiAlC_2 ceramics. It is seen that the sample is very dense and the porosity is extremely rare. The relative density of Mo_2TiAlC_2 ceramics measured by the Archimedes' method was 98.3%, matching well

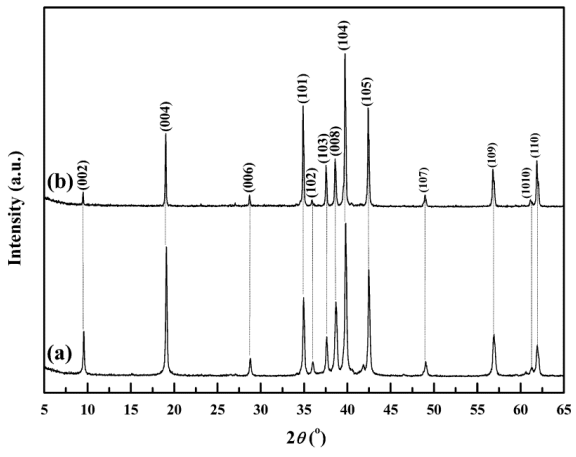

Fig. 2 XRD spectra of (a) dense Mo_2TiAlC_2 bulk sample fabricated by SPS and (b) pure Mo_2TiAlC_2 powder.

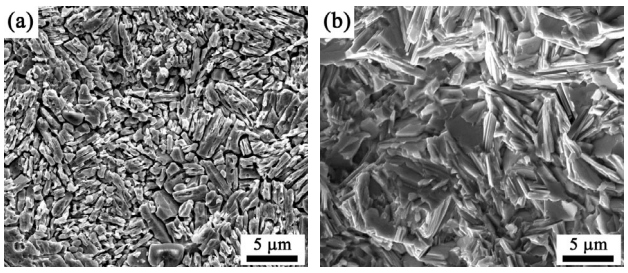

Fig. 3 SEM images of (a) etched surface and (b) fracture surface of dense Mo_2TiAlC_2 ceramics.

with the micrograph. Transgranular fracture and intergranular fracture are the main damage modes. Like other MAX phases, the layered structure of grains could be easily observed, indicating the excellent mechanical properties.

3. 2 Physical and mechanical property evaluation

In order to analyze and describe the properties of Mo_2TiAlC_2 ceramics systematically, the physical and mechanical properties of dense Mo_2TiAlC_2 ceramics were compared to those of Ti_3AlC_2 and $Mo_2Ti_2AlC_3$. In comparison with the property of Ti_3AlC_2, it is easier to investigate the property variation law of the 312 phase whereas the M position atom was partially replaced, which provides a possibility to prepare a new MAX phase according to the intention. The comparison between Mo_2TiAlC_2 and $Mo_2Ti_2AlC_3$ could enrich us with the understanding of the properties of the Mo–Ti–Al–C system MAX phases. Table 2 summarizes the property comparison of $Mo_2Ti_2AlC_3$ and Ti_3AlC_2, including physical properties and mechanical properties [40,51]. Also, the properties of reported Mo_2TiAlC_2 ceramic were added to compare the difference of properties affected by the microstructure [38].

Figure 4 displays the electrical conductivity and electrical resistivity of Mo_2TiAlC_2 at the temperature range of 2–300 K. The electrical conductivity of Mo_2TiAlC_2 measured at room temperature was 0.77×10^6 $\Omega^{-1}\cdot m^{-1}$, which is higher than that of $Mo_2Ti_2AlC_3$ (0.41×10^6 $\Omega^{-1}\cdot m^{-1}$) [40], but lower than that of Ti_3AlC_2 (3.48×10^6 $\Omega^{-1}\cdot m^{-1}$) [51]. In addition, the electrical conductivity of Mo_2TiAlC_2 measured by Anasori *et al*. [38] at 10 K was 0.67×10^6 $\Omega^{-1}\cdot m^{-1}$, lower than the present 0.95×10^6 $\Omega^{-1}\cdot m^{-1}$, which is because of the difference of relative density and content of impurities. The decreasing trend of electrical conductivity from 0.95×10^6 to 0.77×10^6 $\Omega^{-1}\cdot m^{-1}$ can be seen at the temperature range of 2–300 K and indicates a metal-like conductivity from 50 to 300 K with a linear change. Correspondingly, the electrical resistivity increases with the temperature at the range of 2–300 K, similar to other MAX phases. The temperature dependence of electrical (ρ) resistivity can be expressed by

$$\rho\ (\mu\Omega\cdot m) = \rho_0\,(1-\beta\Delta T) = 1.27\,[1 - 0.000717(273.15-T)] \quad (6)$$

where ρ_0 is the electrical resistivity value at 273.15 K ($\mu\Omega\cdot m$), T is the absolute temperature, and β is the temperature coefficient of resistivity (K^{-1}). The value of β is 0.717×10^3 K^{-1}, which is higher than that of $Mo_2Ti_2AlC_3$ (0.324×10^3 K^{-1}) [40], but lower than that of Ti_3AlC_2 (3.10×10^3 K^{-1}) [51].

Table 2 Comparative analysis of physical and mechanical properties of Mo_2TiAlC_2, $Mo_2Ti_2AlC_3$, and Ti_3AlC_2 ceramics

Property	Mo_2TiAlC_2 (this study)	Mo_2TiAlC_2 [38]	$Mo_2Ti_2AlC_3$ [40]	Ti_3AlC_2 [51]
Molecular weight (g/mol)	290.75	290.75	350.63	194.61
Density (g/cm^3)	6.46	5.32	6.15	4.21
Relative density (%)	98.3	81	99.3	99.1
Grain size (μm)	3.5 μm (*L*), 1.0 μm (*W*)	—	5.0 μm (*L*), 1.3 μm (*W*)	~20 μm (*L*), ~10 μm (*W*)
Electrical conductivity (10^6 $\Omega^{-1}\cdot m^{-1}$, 300 K)	0.77	0.48	0.41	3.48
Temperature coefficient of resistivity (10^3 K^{-1})	0.717	—	0.324	3.50
Thermal conductivity ($W\cdot(m\cdot K)^{-1}$, 300 K)	8.0	—	6.82	40
TEC (10^{-6} K^{-1})	9.0 ± 1.5	—	11.3	9.0
Vickers hardness (GPa)	5.20 ± 0.10 (10 N load)	—	4.81 ± 0.15 (10 N load)	2.7 (10 N load)
Flexural strength (MPa)	407.9 ± 29.0	—	452 ± 17	340
Fracture toughness (MPa·m$^{1/2}$)	6.5 ± 0.4	—	8.4 ± 0.4	7.2
Compressive strength (MPa)	1079 ± 17	—	1145 ± 57	764

L: length; *W*: width.

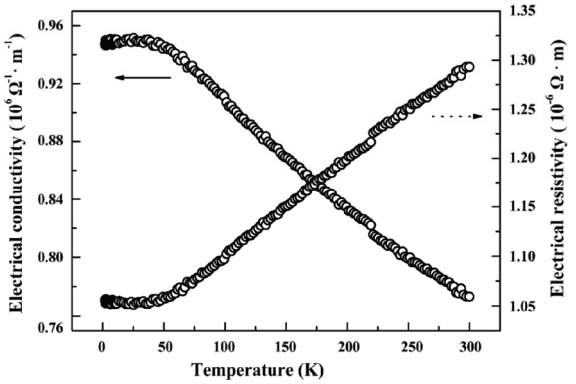

Fig. 4 Electrical conductivity and resistivity of dense Mo_2TiAlC_2 ceramics as a function of temperature.

The thermal conductivity measured at a temperature range of 300–1273 K is shown in Fig. 5. It is seen that the thermal conductivity changes linearly with the increment of temperature, decreasing from 8.0 to 6.4 W·(m·K)$^{-1}$. The thermal conductivity at room temperature is 8.0 W·(m·K)$^{-1}$, which is slightly higher than that of $Mo_2Ti_2AlC_3$ (6.82 W·(m·K)$^{-1}$) [40], and greatly lower than that of Ti_3AlC_2 (40 W·(m·K)$^{-1}$) [51]. A least-square fitting of the temperature dependent thermal conductivity (λ) for Mo_2TiAlC_2 ceramics is described as

$$\lambda = 8.4 - 0.00154T \quad (7)$$

where the coefficient of determination r^2 is 0.99. The trend is similar to those of $Mo_2Ti_2AlC_3$ and Ti_3AlC_2, whose thermal conductivities decrease with the increment of temperature. In addition, the total thermal conductivity can be divided into electronic contribution and phonon contribution, and the relation can be expressed as $\lambda_{total} = \lambda_{electron} + \lambda_{phonon}$. Based on the Wiedmann–Franz Law, the value of $\lambda_{electron}$ can be calculated by the formula of $\lambda_{electron} = L_0\sigma T$, where σ is the electrical conductivity at temperature T, and $L_0 = 2.45 \times 10^{-8}$ W·(m·K)$^{-1}$ [52]. The calculated result of $\lambda_{electron}$ at 300 K is 5.7 W·(m·K)$^{-1}$. Therefore, the contribution of phonon is 2.3 W·(m·K)$^{-1}$ at 300 K.

The TEC of Mo_2TiAlC_2 ceramic measured in the temperature of 350–1100 K is shown in Fig. 6. The simulated line is very fitting to the measured thermal expansion curve. The mean TEC in the temperature range of 350–1100 K was 9.0×10^{-6} K^{-1}, which is the same as that of Ti_3AlC_2 ceramic (9.0×10^{-6} K^{-1}) [51]. Whereas, in comparison with that of the similar $Mo_2Ti_2AlC_3$ ceramic (11.3×10^{-6} K^{-1}) [40], the TEC of Mo_2TiAlC_2 exhibits a lower value, which is probably associated with the stronger bonds in the Mo_2TiAlC_2 crystal structure [38,53].

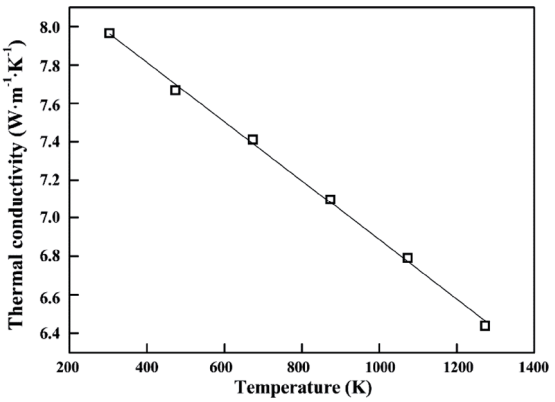

Fig. 5 Thermal conductivity of dense Mo_2TiAlC_2 ceramic as a function of temperature.

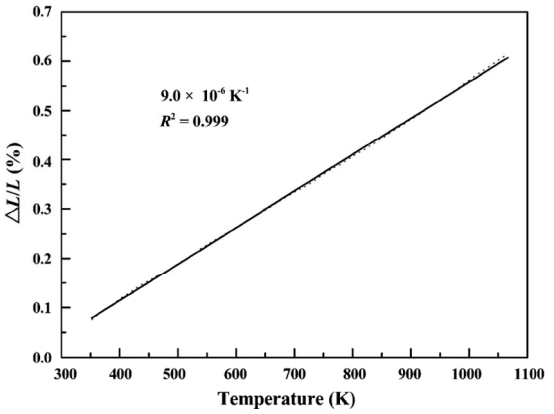

Fig. 6 TEC of dense Mo_2TiAlC_2 ceramic versus temperature.

The Vickers hardness of Mo_2TiAlC_2 ceramics at the load of 10 N was measured as 5.2 ± 0.1 GPa, higher than both $Mo_2Ti_2AlC_3$ of 4.81 GPa [40] and Ti_3AlC_2 of 2.7 GPa [51]. The higher Vickers hardness could be probably ascribed to the SPS method. Fast sintering speed and short holding time contributed to the achievement of small grain size of Mo_2TiAlC_2 ceramics, resulting in the high Vickers hardness. In addition, the Vickers hardness of Mo_2TiAlC_2 as a function of indentation load is displayed in Fig. 7. It is shown that the hardness decreases with increasing load and gradually approaches 5.2 GPa. This phenomenon is well matching the indentation size effect (ISE) of higher hardness at lower loads consisting of the larger elastic recovery [54]. Therefore, the intrinsic hardness value of Mo_2TiAlC_2 ceramic is close to 5.2 GPa. An SEM image of a Vickers indent under a load of 10 N is shown in the inset of Fig. 7. No cracks propagated at the indent diagonals, and similar to other MAX phases, grains crushing, delamination, transgranular, and intergranular fractures were observed around the indent region. The mechanical energy could be effectively

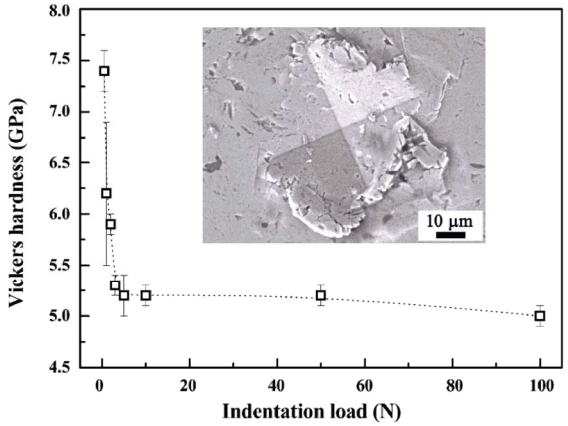

Fig. 7 Vickers hardness of dense Mo_2TiAlC_2 ceramic as a function of indention load. Inset: SEM image of the indent induced by 10 N.

absorbed by these damage modes to prevent stress concentration. As a result, the damage induced by load could be retained in a limited region to keep the integrity of the bulk sample to remain the high strength.

The fracture toughness of Mo_2TiAlC_2 ceramic was tested to be 6.5 ± 0.4 MPa·$m^{1/2}$, lower than both $Mo_2Ti_2AlC_3$ of 8.4 MPa·$m^{1/2}$ [40] and Ti_3AlC_2 of 7.2 MPa·$m^{1/2}$ [51]. Also, Mo_2TiAlC_2 has a high compressive strength up to 1079 ± 17 MPa, a little lower than $Mo_2Ti_2AlC_3$ of 1145 MPa [40], but much higher than Ti_3AlC_2 of 764 MPa [51]. The high compressive strength was contributed by the fine grain size which provides great mechanical properties, including flexural strength. The flexural strength of Mo_2TiAlC_2 is 407.9 ± 29 MPa, higher than that of Ti_3AlC_2 (340 MPa) [51], and a little lower than that of $Mo_2Ti_2AlC_3$ (452 MPa) [40]. In addition, the damage tolerance of Mo_2TiAlC_2 reflected by the indentation load dependence of residual flexural strength is displayed in Fig. 8. At the indentation loads below 200 N, Mo_2TiAlC_2 ceramic can still hold high flexural strength. No obvious strength degradation was observed. When the indentation load was up to 300 N, the residual flexural strength of 343.9 MPa is still about 84% of the strength of undamaged samples. Mo_2TiAlC_2 ceramic possesses a good damage tolerance like Ti_3AlC_2 [55].

3. 3 Oxidation resistance evaluation

Furthermore, to examine the possible application field of Mo_2TiAlC_2 ceramic at high temperatures, the dynamic oxidation process of Mo_2TiAlC_2 ceramics was characterized, as shown in Fig. 9. Figure 9 presents the TG and DSC results of Mo_2TiAlC_2 ceramic measured at the temperature range of 313–1473 K inflowing air. Based on the TG results, it is obviously seen that the mass gain starts at 1070 K and continues to increase until 1200 K, indicating that the sample began to be oxidized. The DSC curve also coincides with this result with an endothermic peak appearing from 1070 K and reaching an extreme value at 1200 K. After 1200 K, the TG curve begins to decrease and the DSC curve begins to turn the direction of heat release. The weight loss is probably associated with the evaporation of MoO_3 because its boiling point is only 1423 K.

To further investigate the oxidation resistance of Mo_2TiAlC_2 ceramics, the bulk sample was oxidized in the tube furnace in the air. The XRD analysis of the sample surface after the oxidizing test from room temperature to 1473 K is shown in Fig. 10. It can be seen that the surface phases are α-Al_2O_3 and R-TiO_2, and no molybdenum oxide MoO_3 peaks were detected. The result is matching the test of TG–DSC well that the MoO_3 phase has completely volatilized at high temperatures. Figure 11 shows the micrograph of the

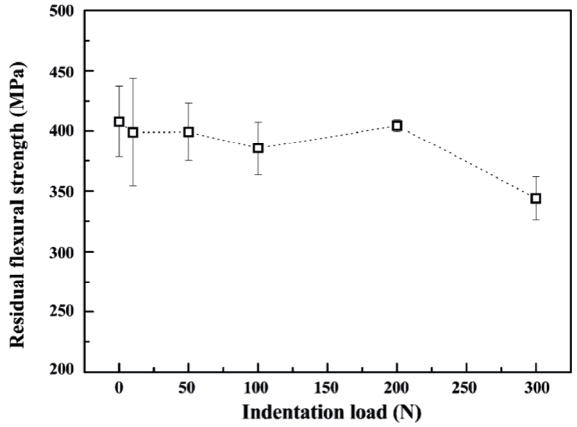

Fig. 8 Indentation load dependence of flexural strength of dense Mo_2TiAlC_2 ceramic, presenting the excellent damage tolerance.

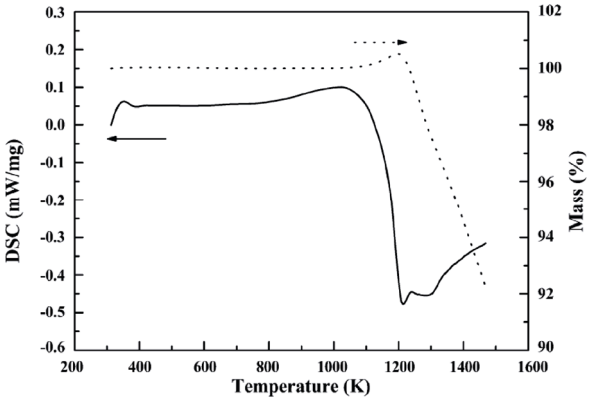

Fig. 9 DSC–TG curves of dense Mo_2TiAlC_2 ceramic as a function of temperature in flowing air.

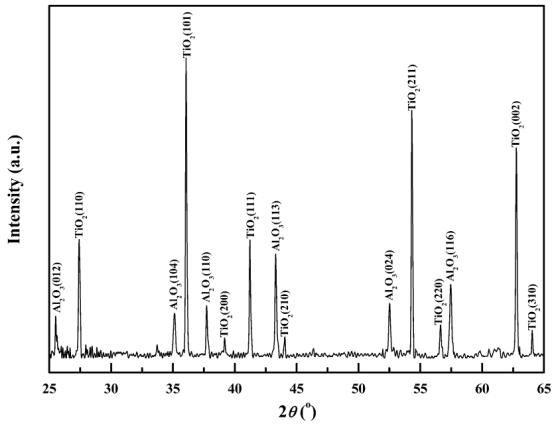

Fig. 10 XRD pattern of oxidized surface of dense Mo_2TiAlC_2 ceramic heat treated in the tube furnace from room temperature to 1473 K in the air.

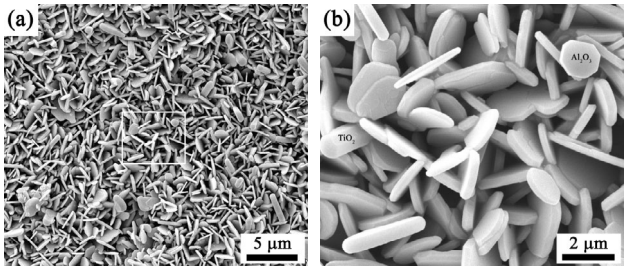

Fig. 11 SEM micrographs of (a) the oxidized surface of dense Mo_2TiAlC_2 ceramic when oxidized from room temperature to 1473 K in the air and (b) the magnified image of the square region in Fig. 11(a).

surface after oxidation. The surface was covered by a loose layer consisting of Al_2O_3 and TiO_2 (Fig. 11(a)). In the magnified image, the hexagonal Al_2O_3 plates and TiO_2 rods could be clearly distinguished (Fig. 11(b)). It seems that different from the oxidized surface of Ti_3AlC_2, no dense oxide layer could be formed on the surface of Mo_2TiAlC_2 ceramic during the oxidation process [28], which presents the poor oxidation resistance above 1473 K. Therefore, it is determined that dense Mo_2TiAlC_2 ceramic could at least endure the high temperature up to 1200 K in the air.

4 Conclusions

In this study, high purity Mo_2TiAlC_2 powder was successfully synthesized by *in situ* reaction and the reaction mechanisms were carefully investigated. Dense bulk Mo_2TiAlC_2 ceramics were consolidated by SPS, and the physical and mechanical properties, as well as oxidation resistance, were systematically studied. The conclusions are listed as follows:

1) High purity Mo_2TiAlC_2 powder could be prepared at 1873 K using Mo, Ti, Al, and C element powders with the molar ratio of 2:1:1.25:2 in the flowing argon. The formation mechanism of Mo_2TiAlC_2 was ascribed to the reaction among Mo_3Al_2C, Mo_2C, TiC, and C.

2) The SPSed dense Mo_2TiAlC_2 ceramics with a high relative density of 98.3% had the fine grain size of 3.5 μm in length and 1.0 μm in width. The electrical conductivity measured at room temperature was 0.77×10^6 $\Omega^{-1}\cdot m^{-1}$, and it tended to increase with the decreasing temperature. When the temperature reached 2 K, the electrical conductivity increased to be 0.95×10^6 $\Omega^{-1}\cdot m^{-1}$. The thermal conductivity measured in the temperature of 300–1273 K decreased from 8.0 to 6.4 $W\cdot(m\cdot K)^{-1}$, and TEC measured in the temperature of 350–1100 K was 9.0×10^{-6} K^{-1}.

3) Dense Mo_2TiAlC_2 ceramic had the low intrinsic Vickers hardness of 5.2 GPa, high fracture toughness of 6.5 $MPa\cdot m^{1/2}$, high compressive strength of 1079 MPa, and high flexural strength of 407.9 MPa. When the indent load was up to 300 N, the residual flexural strength could still hold 84% of the value of the undamaged sample, presenting excellent damage tolerance.

4) The oxidation resistance of dense Mo_2TiAlC_2 ceramics could retain up to 1200 K in the air, presenting the potential application in the high-temperature fields.

Acknowledgements

This study was supported by the Thousand Talents Program of Sichuan Province, the Open Project of State Key Laboratory Cultivation Base for Nonmetal Composites and Functional Materials (17kffk01), the Outstanding Young Scientific and Technical Talents in Sichuan Province (2019JDJQ0009), and the National Natural Science Foundation of China (Nos. 51741208 and 52072311).

References

[1] Li X, Liang BY, Li ZX. Combustion synthesis of Ti_2SC. *Int J Mater Res* 2013, **104**: 1038–1040.

[2] Tunca BS, Lapauw T, Karakulina OM, *et al*. Synthesis of MAX phases in the Zr–Ti–Al–C system. *Inorg Chem* 2017, **56**: 3489–3498.

[3] Mockute A, Dahlqvist M, Emmerlich J, *et al*. Synthesis and *ab initio* calculations of nanolaminated $(Cr,Mn)_2AlC$ compounds. *Phys Rev B* 2013, **87**: 094113.

[4] Lapauw T, Lambrinou K, Cabioc'H T, *et al*. Synthesis of the new MAX phase Zr_2AlC. *J Eur Ceram Soc* 2016, **36**: 1847–1853.

[5] Lapauw T, Halim J, Lu J, *et al*. Synthesis of the novel Zr_3AlC_2 MAX phase. *J Eur Ceram Soc* 2016, **36**: 943–947.
[6] Gauthier-Brunet V, Cabioc'H T, Chartier P, *et al*. Reaction synthesis of layered ternary Ti_2AlC ceramic. *J Eur Ceram Soc* 2009, **29**: 187–194.
[7] Dubois S, Bei GP, Tromas C, *et al.* Synthesis, microstructure, and mechanical properties of $Ti_3Sn_{(1-x)}Al_xC_2$ MAX phase solid solutions. *Int J Appl Ceram* 2010, **7**: 719–729.
[8] Opeka M, Zaykoski J, Talmy I, *et al.* Synthesis and characterization of Zr_2SC ceramics. *Mat Sci E A-Struct* 2011, **528**: 1994–2001.
[9] Faraoun HI, Abderrahim FZ, Esling C. First principle calculations of MAX ceramics Cr_2GeC, V_2GeC and their substitutional solid solutions. *Comput Mater Sci* 2013, **74**: 40–49.
[10] Wang Q, Hu CF, Cai S, *et al.* Synthesis of high purity Ti_3SiC_2 by microwave sintering. *Int J Appl Ceram Tec* 2014, **11**: 911–918.
[11] Saeed MA, Deorsola FA, Rashad RM. Optimization of the Ti_3SiC_2 MAX phase synthesis. *Int J Refract Met H* 2012, **35**: 127–131.
[12] Li SB, Zhai HX. Synthesis and reaction mechanism of Ti_3SiC_2 by mechanical alloying of elemental Ti, Si, and C powders. *J Am Ceram Soc* 2005, **88**: 2092–2098.
[13] Yan M, Chen YL, Mei BC, *et al.* Synthesis of high-purity Ti_2AlN ceramic by hot pressing. *T Nonferr Metal Soc* 2008, **18**: 82–85.
[14] Liu Y, Zhang LL, Xiao WW, *et al*. Rapid synthesis of Ti_2AlN ceramic via thermal explosion. *Mater Lett* 2015, **149**: 5–7.
[15] Zhu JF, Gao JQ, Yang JF, *et al*. Synthesis and microstructure of layered-ternary Ti_2AlC ceramic by high energy milling and hot pressing. *Mater Sci Eng: A* 2008, **490**: 62–65.
[16] Hu CF, Zhou YC, Bao YW. Material removal and surface damage in EDM of Ti_3SiC_2 ceramic. *Ceram Int* 2008, **34**: 537–541.
[17] Rawn C, Barsoum M, El-Raghy T, *et al*. Structure of Ti_4AlN_3—A layered $M_{n+1}AX_n$ nitride. *Mater Res Bull* 2000, **35**: 1785–1796.
[18] Zhou YC, Sun ZM. Microstructure and mechanism of damage tolerance for Ti_3SiC_2 bulk ceramics. *Mater Res Innov* 1999, **2**: 360–363.
[19] Barsoum MW, Yoo HI, Polushina IK, *et al*. Electrical conductivity, thermopower, and Hall effect of Ti_3AlC_2, Ti_4AlN_3, and Ti_3SiC_2. *Phys Rev B* 2000, **62**: 10194.
[20] El-Raghy T, Zavaliangos A, Barsoum MW, *et al*. Damage mechanisms around hardness indentations in Ti_3SiC_2. *J Am Ceram Soc* 2005, **80**: 513–516.
[21] Lai CC, Petruhins A, Lu J, *et al*. Thermally induced substitutional reaction of Fe into Mo_2GaC thin films. *Mater Res Lett* 2017, **5**: 533–539.
[22] Amini S, Zhou AG, Gupta S, *et al*. Synthesis and elastic and mechanical properties of Cr_2GeC. *J Mater Res* 2008, **23**: 2157–2165.
[23] Lin ZJ, Zhou YC, Li MS. Synthesis, microstructure, and property of Cr_2AlC. *J Mater Sci Tech* 2007, **13**: 721–746.
[24] Li XC, Zheng LL, Qian YH, *et al*. Breakaway oxidation of Ti_3AlC_2 during long-term exposure in air at 1100 ℃. *Corros Sci* 2016, **104**: 112–122.
[25] Wang XH, Zhou YC. Oxidation behavior of Ti_3AlC_2 at 1000–1400 ℃ in air. *Corros Sci* 2003, **45**: 891–907.
[26] Qian XK, He XD, Li YB, *et al*. Cyclic oxidation of Ti_3AlC_2 at 1000–1300 ℃ in air. *Corros Sci* 2011, **53**: 290–295.
[27] Tallman DJ, Anasori B, Barsoum MW. A critical review of the oxidation of Ti_2AlC, Ti_3AlC_2 and Cr_2AlC in air. *Mater Res Lett* 2013, **1**: 115–125.
[28] Wang XH, Zhou YC. Layered machinable and electrically conductive Ti_2AlC and Ti_3AlC_2 ceramics: A review. *J Mater Sci Technol* 2010, **26**: 385–416.
[29] Amini S, Barsoum MW, El-Raghy T. Synthesis and mechanical properties of fully dense Ti_2SC. *J Am Ceram Soc* 2007, **90**: 3953–3958.
[30] Hu CF, He LF, Zhang J, *et al.* Microstructure and properties of bulk Ta_2AlC ceramic synthesized by an *in situ* reaction/hot pressing method. *J Eur Ceram Soc* 2008, **28**: 1679–1685.
[31] Hu CF, He LF, Liu MY, *et al*. *In situ* reaction synthesis and mechanical properties of V_2AlC. *J Am Ceram Soc* 2008, **91**: 4029–4035.
[32] Sun ZM, Music D, Ahuja R, *et al*. Electronic origin of shearing in M_2AC (M = Ti, V, Cr, A = Al, Ga). *J Phys: Condens Matter* 2005, **17**: 7169–7176.
[33] Music D, Schneider JM. The correlation between the electronic structure and elastic properties of nanolaminates. *JOM* 2007, **59**: 60–64.
[34] Lin ZJ, Zhou YC, Li MS, *et al*. *In-situ* hot pressing/solid–liquid reaction synthesis of bulk Cr_2AlC. *Zeitschrift Für Met* 2005, **96**: 291–296.
[35] Wang J, Zhou Y. Dependence of elastic stiffness on electronic band structure of nanolaminate M_2A1C (M = Ti, V, Nb, and Cr) ceramics. *Phys Rev B* 2004, **69**: 214111.
[36] Zhou YC, Meng FL, Zhang J. New MAX-phase compounds in the V–Cr–Al–C system. *J Am Ceram Soc* 2008, **91**: 1357–1360.
[37] Zheng LY, Wang JM, Lu XP, *et al*. $(Ti_{0.5}Nb_{0.5})_5AlC_4$: A new-layered compound belonging to MAX phases. *J Am Ceram Soc* 2010, **93**: 3068–3071.
[38] Anasori B, Dahlqvist M, Halim J, *et al*. Experimental and theoretical characterization of ordered MAX phases Mo_2TiAlC_2 and $Mo_2Ti_2AlC_3$. *J Appl Phys* 2015, **118**: 094304.
[39] Anasori B, Halim J, Lu J, *et al*. Mo_2TiAlC_2: A new ordered layered ternary carbide. *Scripta Mater* 2015, **101**: 5–7.
[40] Fu S, Liu YL, Zhang HW, *et al*. Synthesis and characterization of high purity $Mo_2Ti_2AlC_3$ ceramic. *J Alloys Compd* 2020, **815**: 152485.
[41] Omori M. Sintering, consolidation, reaction and crystal growth by the spark plasma system (SPS). *Mater Sci Eng: A* 2000, **287**: 183–188.
[42] Mamedov V. Spark plasma sintering as advanced PM

sintering method. *Powder Metall* 2002, **45**: 322–328.
[43] Wang YC, Fu ZY. Study of temperature field in spark plasma sintering. *Mater Sci Eng: B* 2002, **90**: 34–37.
[44] Tokita M. Trends in advanced SPS Spark Plasma Sintering systems and FGM technology. *J S Power Tech* 1993, **30**: 790–804.
[45] Parrikar PN, Gao HL, Radovic M, *et al.* Static and dynamic thermo-mechanical behavior of Ti_2AlC MAX phase and fiber reinforced Ti_2AlC composites. In *Dynamic Behavior of Materials*. Song B, Casem D, Kimberley J, Eds. Cham: Springer International Publishing, 2015, **1**: 9–14.
[46] Choi ES, Sung J, Wang QM, *et al*. Material properties and machining performance of hybrid Ti_2AlN bulk material for micro electrical discharge machining. *Trans Nonferrous Met Soc China* 2012, **22**: 781–786.
[47] Griseri M, Tunca BS, Lapauw T, *et al*. Synthesis, properties and thermal decomposition of the Ta_4AlC_3 MAX phase. *J Eur Ceram Soc* 2019, **39**: 2973–2981.
[48] Lapauw T, Vanmeensel K, Lambrinou K, *et al*. Rapid synthesis and elastic properties of fine-grained Ti_2SnC produced by spark plasma sintering. *J Alloys Compd* 2015, **631**: 72–76.
[49] Duan XM, Shen L, Jia DC, *et al.* Synthesis of high-purity, isotropic or textured Cr_2AlC bulk ceramics by spark plasma sintering of pressure-less sintered powders. *J Eur Ceram Soc* 2015, **35**: 1393–1400.
[50] Liu Y, Li YX, Li F, *et al*. Highly textured Ti_2AlN ceramic prepared via thermal explosion followed by edge-free spark plasma sintering. *Scripta Mater* 2017, **136**: 55–58.
[51] Wang X, Zhou Y. Microstructure and properties of Ti_3AlC_2 prepared by the solid–liquid reaction synthesis and simultaneous *in-situ* hot pressing process. *Acta Mater* 2002, **50**: 3143–3151.
[52] Barsoum MW, Rawn CJ, El-Raghy T, *et al*. Thermal properties of Ti_4AlN_3. *J Appl Phys* 2000, **87**: 8407–8414.
[53] Li YF, Xiao B, Sun L, *et al*. Phonon spectrum, IR and Raman modes, thermal expansion tensor and thermal physical properties of M_2TiAlC_2 (M = Cr, Mo, W). *Comput Mater Sci* 2017, **134**: 67–83.
[54] Hu CF, Lin ZJ, He LF, *et al*. Physical and mechanical properties of bulk Ta_4AlC_3 ceramic prepared by an *in situ* reaction synthesis/hot-pressing method. *J Am Ceram Soc* 2007, **90**: 2542–2548.
[55] Gong YM, Tian WB, Zhang PG, et al. Slip casting and pressureless sintering of Ti_3AlC_2. *J Adv Ceram* 2019, **8**: 367–376.